Influence of non-aqueous phase liquid configuration on induced polarization parameters: conceptual models applied to a time-domain field case study

Sara Johansson[1], Gianluca Fiandaca[2], Torleif Dahlin[1]

1. Engineering Geology, Lund University, P.O. Box 118, SE-22100, Lund, Sweden

2. Department of Geoscience, Aarhus University, C.F.Møllers Allé 4, building 1120, 8000 Aarhus C, Denmark

Corresponding author: Sara Johansson, sara.johansson@tg.lth.se, +46 46 222 74 23, Engineering Geology, Lund University, P.O. Box 118, SE-22100, Lund, Sweden

ABSTRACT

Resistivity and induced polarization (IP) measurements on soil contaminated with Non-Aqueous Phase Liquids (NAPL) show a great variety in results in previous research. Several laboratory studies have suggested that the presence of NAPLs in soil samples generally decrease the magnitude of the IP-effect, while others have indicated the opposite. A number of conceptual models have been proposed suggesting that NAPLs can alter the pore space in different ways, e.g. by coating the grain surfaces and thus inhibiting grain polarization, or by changing the pore throat size and thus affecting the membrane polarization mechanism. The main aim of this paper is to review previously published conceptual models and to introduce some new concepts of possible residual NAPL configurations in the pore space. Time domain induced polarization measurements were performed at a NAPL contaminated field site, and the data were inverted using the Constant Phase Angle (CPA) model and the Cole-Cole model respectively. No significant phase anomalies were observed in the source area of the contamination when the CPA inverted profiles were compared with soil sampling results of free-phase contaminant concentrations. However, relatively strong phase and normalized phase anomalies appeared next to the source area, where residual free-phase presence could be expected according to the chemical data. We conclude that depending on the NAPL configuration, different spectral IP responses can be expected. In previous research, the NAPL configurations in different samples or field sites are often unknown, and this may to some extent explain

why different results have been achieved by different authors. In our field case, we believe that the NAPL forms a more or less continuous phase in the pore space of the source zone leading to an absence of IP anomalies. The increase in phase and normalized phase angle observed next to the source zone is interpreted as a degradation zone. The ongoing biodegradation may have led to a fractionation of the continuous NAPL in the outer part of the original source zone, leading to residual presence of isolated NAPL droplets in the soil pores. With such NAPL configurations, an increased polarization can be expected according to the electrochemical- and membrane polarization mechanisms. More research is needed to confirm the effects of different NAPL configuration on spectral IP parameters.

1. INTRODUCTION

A common environmental problem is the remediation of ground contaminated with Non-Aqueous Phase Liquids (NAPLs), e.g. gasoline or industrial chlorinated solvents. These chemicals are immiscible liquids that do not easily dissolve in water, and as such they often exist as an own phase in the soil (a so called free-phase product). NAPLs are divided into light non-aqueous phase liquids (LNAPLs) and dense non-aqueous phase liquids (DNAPLs), where the former have a lower density and the latter have a higher density than water. The density difference has the implication that large LNAPL spills are often found floating on the groundwater surface when released into the ground, while DNAPLs sink trough the groundwater until it reaches a less permeable layer, e.g. the bedrock. Free-phase products of both LNAPLs and DNAPLs can exist as a continuous phase in the ground or as a residual phase, where parts of the contaminant have been trapped in the soil and are not displaced due to gravitational forces (Atekwana & Atekwana 2010; Ajo-Franklin et al. 2006).

Delineations of NAPL plumes are commonly carried out by means of borehole drilling and chemical sampling. However, there is a risk of spreading the contaminants vertically during this process and the drillings are expensive and give point information rather than a continuous picture of the contaminant plume. Geophysical methods are, in a general sense, effective tools in providing continuous information of soil properties in between individual boreholes. Resistivity and induced polarization (IP) are methods that have been considered promising in order to achieve detection of NAPLs in soils, and research has been

carried out in both laboratory and field. The interest in the resistivity method has emerged because NAPLs are electrical insulators and can cause a rise in resistivity when their free-phase products displace water in saturated soil. This has been observed in a number of lab and field studies on different kinds of NAPLs (e.g. Chambers et al. 2004; Cassiani et al. 2009; Naudet et al. 2014; Power et al. 2015). However, at field sites, the situation is complicated by the fact that the age and degradation status of the contaminants change the groundwater chemistry. Release of ions during biodegradation, or mineral weathering and dissolution caused by organic acids released by bacteria, can cause increased groundwater conductivity (Atekwana & Slater 2009; Atekwana & Atekwana 2010). Thus, increased bulk resistivity due to free-phase NAPL presence could be suppressed by increased groundwater conductivity.

A possible solution to the problem of using resistivity alone for NAPL detection is to extend the measurements to include IP. IP spectra or time decays are sensitive to properties at the pore scale, such as e.g. grain sizes, grain shape, grain surface chemistry and pore throat size distribution (e.g. Slater & Lesmes 2002; Scott & Barker 2003; Binley et al. 2005; Nordsiek & Weller 2008; Titov et al. 2010). Consequently, the IP method may have a greater potential of being able to detect NAPLs in the pore space compared to resistivity alone. However, the results of previous studies in both field and laboratory scale vary and sometimes point in opposite directions. Several laboratory measurements have suggested that the presence of NAPLs in water saturated soil samples generally reduce the magnitude of the IP effect (Börner et al. 1993; Vanhala et al. 1992; Vanhala 1997; Chambers et al. 2004; Martinho et al. 2006; Schmutz et al. 2010; Revil et al. 2011), while others have indicated the opposite (Olhoeft 1985; Titov et al. 2004; Cassiani et al. 2009; Schmutz et al. 2010; Schmutz et al. 2012). As expected, varied results have also been achieved in field surveys of NAPL contaminated ground. For example, free-phase NAPL presence in an unconfined aquifer have resulted in decreased chargeability (Flores Orozco et al. 2012), while in another field study, high chargeability was interpreted as an indicator of LNAPLs in clayey sand (Deceuster & Kaufmann 2012).

In contrast to several lab studies, where the relationship between NAPL concentration and IP response has been interpreted as essentially linear (e.g. Schmutz 2010, Revil 2011, Schmutz 2012), other trends have also been observed. In some cases, a threshold value in the relationship between NAPL concentration and IP response in water saturated soil samples has been seen. Titov et al. (2004) found increasing chargeability

79 with LNAPL content up to a saturation of 92% and decreasing chargeability with further increase of the
80 LNAPL. A similar trend have been observed by Schmutz et al. (2012). In contrast, measurements by
81 Martinho et al. (2006) indicated an initial decrease of chargeability values up to a LNAPL saturation of
82 around 10% in clayey sand samples. Slightly increasing chargeability values were observed at higher
83 contents, although all values were below the values of clean sand, in contrast to the data from Titov et al.
84 (2004).

85 It is not always straightforward to compare the results from previous laboratory measurements since there
86 can be variations in e.g. sample preparation and NAPL phases and species (Cassiani et al. 2009). Field data
87 is often even more challenging because of different field circumstances such as geological setting and
88 degradation status. Beyond variations in chemical, biological and geological parameters, a factor that plays
89 a major role in understanding the effect on measured IP of NAPL in soils is the geometrical configuration of
90 the free-phase product in the pore space. In published research, interpretation of IP data often rely on
91 different conceptual models of NAPL configuration, which in different ways explain the observed results
92 (e.g. Olhoeft 1985; Titov et al. 2004; Martinho et al. 2006; Schmutz et al. 2010; Revil et al. 2011; Flores
93 Orozco et al. 2012; Shefer et al. 2013). However, to date, there are no comparative studies discussing
94 possible effects of different models. There is thus a need for a comprehensive discussion and comparison
95 of various possible NAPL configurations, since this may enhance the understanding of why different results
96 may be achieved when IP measurements are performed on NAPL contaminated soil.

97 The main aim of this paper is to review previously published conceptual models and to introduce some new
98 concepts of possible residual NAPL configurations in the pore space. We will discuss how the conceptual
99 models can be expected to influence spectral (Cole-Cole) IP parameters (section 5). Field results from time
100 domain IP measurements on a site contaminated with DNAPLs will be presented (section 4) and discussed
101 in relation to the qualitative results from the discussion of NAPL configurations. The data were inverted
102 with both the Constant Phase Angle (CPA) model and the Cole-Cole model. The results indicate a zone of
103 increased phase/chargeability and decreased relaxation time at a location outside the free-phase source
104 area, while no effects can be distinguished at the locations where the highest DNAPL concentrations were
105 observed. The increased IP effects are interpreted as possible effects of residual free-phase presence. We

106 believe that the concentration and configuration of the DNAPL in the soil are important since this will affect
107 the micro geometrical properties at the pore scale and the current paths through the soil.

108 In a wider context, we wish to raise the awareness of the importance of assumptions about the NAPL
109 configuration in a pore space, an issue that was also stressed by Cassiani et al. (2009), and its possible
110 impacts on spectral IP parameters. We believe that such considerations could enhance future
111 interpretations of IP data measured on NAPL contaminated lab samples or field sites.

112 **2. THEORY**

113 ***2.1 POLARIZATION MECHANISMS***

114 The mechanisms behind the spectral induced polarization response in metal-free soils are usually described
115 in terms of electrochemical polarization, membrane polarization or Maxwell-Wagner polarization. The basis
116 of the electrochemical polarization mechanism (also called grain polarization or Stern layer polarization) is
117 the existence of electrical double layers (EDLs) around soil grains. The EDLs arises as a result of a negative
118 surface charge on mineral grains surrounded by water, which leads to attachment of a fixed layer of
119 counter-ions at the grain surface, the so called Stern layer. In addition, a second layer of counter-ions, called
120 the diffuse layer, is formed and consists of more weakly electrostatically attracted solvent ions. When an
121 electrical field is applied to the soil, the EDL becomes polarized (Schwarz 1962). Modelling studies have
122 shown that the polarization of the Stern layer is much stronger in magnitude compared to the polarization
123 of the diffuse layer (de Lima & Sharma 1992; Lesmes & Morgan 2001; Leroy et al. 2008). The total
124 polarization magnitude has been observed to be inversely proportional to the grain size of silts, sands and
125 tills (Slater 2002). The relaxation time increases with the characteristic grain (or pore throat) size, since this
126 determine the possible length scale of diffusion for ions in the EDL (Slater 2007).

127 The concept behind membrane polarization is that series of small ion-selective and non-selective zones
128 exist in the pore system. The ion-selective zones can consist of negatively charged clay particles attracting
129 a cloud of counter-ions, or narrow pores or pore-throats which to a large degree are occupied by the EDLs
130 of the surrounding grains. When an electric field is applied to the system, ions are blocked in front of the

ion-selective zones, and ions attached to mineral particles are displaced. The length ratio and relative ion transparencies between the ion-selective and non-selective zones determines the polarization magnitude, while the length of the non-selective zones controls the diffusion length scale and therefore the relaxation time (Marshall & Madden 1959; Vinegar & Waxman 1984; Titov et al. 2002).

The Maxwell-Wagner polarization mechanism is related to ion accumulations at borders between soil phases with different dielectrical properties, e.g. water and grains. This mechanism dominates at higher frequencies (above 1 kHz) and is also dependent on the shapes of different phases in a soil matrix (Lesmes & Morgan 2001). Quantification of the mechanism requires modelling with effective media theories, and this has usually been made with two-phase systems (de Lima & Sharma 1992; Lesmes & Morgan 2001; Leroy & Revil 2009).

The IP effects measured in a natural soil likely consist of several superposed relaxation mechanisms, but no unifying theory covering interactions between all of the polarization mechanisms is available to date. Therefore, we will discuss both electrochemical and membrane polarization mechanisms in section 5. Although Maxwell-Wagner effects are also likely to influence measured IP effects, this mechanism will not be further discussed. A study of the behavior of the Maxwell-Wagner effect in NAPL contaminated soil requires modeling of three-phase systems, and its behavior cannot be qualitatively predicted from simplified conceptual models as those that will be presented in section 5. Furthermore, we are mainly interested in low-frequency mechanisms.

2.2 FREQUENCY DOMAIN AND TIME DOMAIN IP

In frequency domain, the amplitude- and phase-shifts of an alternating current (AC) that has travelled through a soil volume is measured. The total complex conductivity σ^* (the reciprocal of complex resistivity ρ^*) can be expressed as:

$$\sigma^* = |\sigma| e^{i\phi} \quad (1)$$

where $|\sigma|$ (S/m) is the measured magnitude of the amplitude and ϕ $(mrad)$ is the phase angle.

In time domain, resistivity is measured during the injection of a direct current (DC) pulse, while chargeability is measured as the remaining potential after the current has been switched off. The intrinsic chargeability is defined as (Seigel 1959):

$$m = \frac{V_S}{V_P} \quad (2)$$

where V_p is the primary voltage of the transmitted DC current and V_s is the maximum voltage immediately after the interruption of the current pulse. In practice, m is commonly measured and calculated as the integral of the decay curve during a defined time window (m_i):

$$m_i = \frac{1}{t(i+1)-t(i)} \int_{t(i)}^{t(i+1)} \frac{V dt}{V_p} \quad (3)$$

The complex conductivity (Equation 1) can be rewritten in Cartesian coordinates:

$$\sigma^* = \sigma' + i\sigma'' \quad (4)$$

Where σ' and σ'' are the real and imaginary parts of σ^*, which can be calculated as functions of both $|\sigma|$ and ϕ. The real part σ' represents the electrical conduction in the soil, which is mainly made up of ionic conduction in the groundwater and surface conduction along interconnected grains. The imaginary part σ'' represents the complex and frequency-dependent capacitive properties in the soil, i.e. it is usually assumed to be a measure of the induced polarization effect only. The time domain parameter m can be compared to the frequency domain ϕ, that is, it is affected not only by polarization mechanisms but also the bulk conductivity in the ground. The time domain equivalent to the frequency domain parameter σ'' is called the normalized chargeability (MN) and is calculated by a division with resistivity. Since the normalized parameters (during the right soil conditions, e.g. water saturated and metal free soil) can be assumed to be a measure of the IP effect alone, they are more sensitive to surface chemical properties of the material compared to m and ϕ (Slater & Lesmes 2002).

A number of phenomenological models exist which can be fitted to the IP spectra, among which the most commonly used are the Cole-Cole like model (Cole & Cole 1941; Pelton et al. 1978) and the Constant Phase Angle (CPA) model (e.g. Van Voorhis et al. 1973). The Cole-Cole model assumes a peak frequency of the

polarization spectra and implies four parameters describing the shape of the IP spectra. The Cole-Cole model describing the complex resistivity $\rho^*(\omega)$ is:

$$\rho^*(\omega) = \rho\left[1 - m_0\left(1 - \frac{1}{1+(i\omega\tau)^c}\right)\right] \quad (5)$$

where ρ (Ωm) is the DC resistivity, m_0 $(mV/V)$is the chargeability as defined in (2), τ (s) is the relaxation time, c is the frequency factor, ω (rad) is the angular frequency and i is the imaginary unit (Pelton et al. 1978; Fiandaca et al. 2013). The response of soils or rocks with little or no frequency dependence of the phase shift is often described in frequency domain with the CPA model:

$$\rho^*(\omega) = K(i\omega)^{-b} \quad (6a)$$

in which the phase of the complex resistivity is constant over frequency

$$\phi = -\frac{\pi}{2}b \quad (6b)$$

In the CPA model the modulus of the resistivity increases indefinitely for decreasing frequencies, and it is not possible to define a zero-frequency value, that can instead be defined in the Drake model (Van Voorhis et al. 1973):

$$\rho^*(\omega) = K(i\omega + \omega_l)^{-b} \quad (7a)$$

in which the low-frequency pole ω_l allows the definition of a zero-frequency resistivity ρ

$$\rho = \rho^*(0) = K(\omega_l)^{-b} \quad (7b)$$

The Drake model and the CPA model coincide for $\omega \gg \omega_l$. In the present study when inverting for the CPA model we actually use a Drake model with low-frequency pole ω_l fixed to a small value (1 μHz). In this way we can invert directly for ϕ and ρ, instead of having to invert for the non-conventional parameter K of equation 6a.

3. METHODS & MATERIALS

Resistivity and time domain IP (DCIP) were measured over a former dry-cleaning site in southern Sweden, where a large amount of tetrachloroethylene (PCE) was released between the early 1900s and the late 1980s. The site, which is one of the worst PCE contaminated areas in Sweden, rests on top of a major drinking aquifer, and a protected wetland is situated east of the property boundary, see Figure 1.

The site and its surroundings have previously been extensively investigated with drilling and soil- and groundwater sampling in order to try to delineate the source area of the PCE spill as well as polluted groundwater plumes. While the source area of free-phase PCE resides within the boundaries of the former dry-cleaning site (Figure 1), contaminated groundwater with dissolved degradation products have been widely spread over surrounding areas covering several hectares.

Figure 1. Satellite image of the investigated site with the positions of the DCIP electrodes. The yellow and red markers represents previously drilled boreholes with geological classifications and chemical sampling data respectively.

3.1 PREVIOUS INVESTIGATIONS

The main aim of the DCIP survey was to investigate if the source area of free-phase PCE could be detected with DCIP. As reference data, geological classifications from the previous drilling investigations carried out in between 2008 and 2013 were used. The labelled boreholes in Figure 1 were drilled during the period 2008 to 2010, using auger (100-series) and sonic (500- and 600-series) drilling methods respectively. Polyethene (PEH) wells were installed in approximately every second of the 100- and 500-series boreholes, but these had been removed at the time of the DCIP survey.

A principal sketch of the geological profile across the site is shown in Figure 2. The general geological setting consists mainly of sandy chalk till above a bedrock of sandy limestone. At the southeastern (SE) boundary of the site, the bedrock is situated below -15 mamsl, tilting towards the northwest (NW) to below -20 mamsl. Above the till is a layer of varved clay and a thin layer of fill material. In the NW half of the site, the thickness of the clay layer increases and the clay is interspersed with layers of sand, peat and gyttja clay as the wetland is approached.

Figure 2. Principal geological profile across the site, based on geological classifications from the boreholes in Figure 1. The estimated extension of the free-phase contamination is also shown.

Figure 2 also show a sketch of the estimated vertical extension of the PCE source contamination. The sketch is based on chemical soil sampling results (700-series, Figure 3) performed less than a month before the DCIP measurements in 2013. The soil samples were collected from complete cores extracted from the boreholes with sonic drilling. Shortly after the core drillings, the cores were geologically classified and soil samples were taken out from different levels along the cores and sent for chemical analysis of different chlorinated hydrocarbon species. Generalized results of the chemical analyses are shown in Figure 3, where interpolated spatial extensions and total measured amounts of PCE and its degradation product Cis-1,2-dichlorethene (Cis-1,2-DE) in the sandy chalk till (-4 to -14 mamsl) are visualized. The amounts of Cis-1,2-DE were more than 10 times higher than the first- and third order degradation products trichloroethylene (TCE) and vinyl chloride (VC), which are not visualized in Figure 3.

The interpolated PCE surface in Figure 3 show the probable source area of the contamination, while the Cis-1,2-DE results indicate a main degradation zone east of the source area. High amounts of PCE and Cis-1,2-DE were also found in the upper fill- and clay layers (above -4 mamsl), as qualitatively shown in Figure 2.

No groundwater wells were installed during the drilling campaign 2013 (700-series). Therefore, no reference data on groundwater chemistry at the site were available to compare with the DCIP results. However, divers installed in surrounding areas showed that the groundwater level was located at around -1.7 mamsl during the time of the DCIP measurements.

Figure 3. Summarizing results from the chemical analyses of soil samples taken in the sandy chalk till (below -4 mamsl). The interpolated PCE surface show approximately the main location of the source contamination, while the interpolated Cis-1,2-DE surface indicate the main degradation zone.

3.2 DCIP MEASUREMENTS

Nine parallel DCIP lines separated by 2.5 meters were used to cover the site of the former dry cleaning facility (Figure 1 and Figure 3). The DCIP measurements were made with ABEM Terrameter LS by use of pole-dipole configuration, with an electrode spacing of 2.5m and an average profile length of 80 meters. In order to reduce capacitive coupling, a separated cable layout was used (Dahlin & Leroux 2012). The pole-dipole configuration was used in order to gain good depth penetration in relation to the rather limited spreads, where the spread lengths were limited by the urban character of the site. An electrode spread of 80 metres resulted in maximum median depth penetration of around 30 m, but as the data cover for the deepest levels is limited, the model results for the largest depths were not considered in the interpretation.

Stainless steel electrodes were used for current transmission as well as potential measurements (Dahlin et al. 2002; LaBrecque & Daily 2008). The measurement protocols were designed to avoid using an electrode for potential measurement immediately or soon after it was used for transmitting current, in order to reduce background potential variation due to charge-up during current injection (Dahlin 2000). Attention was devoted to securing good galvanic contact between the electrodes and ground in order to optimise data quality, where a starch based gel (Revert Optimum from Johnson Screens®) proved effective for reducing the contact resistance in coarse grained soils and fill material. Average contact resistances were thereby kept well below 1 kohm with occasional electrodes going up to a few kohm.

A square-wave with 1 second on- and off time was used for the measurements and full-waveform data was recorded. Logarithmically spaced IP gates were integrated over multiples of 60ms to account for and remove train traffic disturbances at 16 2/3 Hz. The total measuring time of each decay curve was 1s, which together with the gating provided a time domain data range corresponding to approximately 1.25 – 25Hz in frequency domain.

3.3 DATA PROCESSING AND INVERSION

The raw data was affected by urban noise but were still of an overall adequate quality. The data sets were processed, and the noisiest decay curves were removed together with some early data points which

indicated coupling effects. Around 25 % of the measured decay curves were removed due to low data quality.

The processed DC and full decay IP data were inverted in 2D with AarhusInv (Auken et al. 2014), following (Fiandaca et al. 2013), with both the CPA and the Cole-Cole models. In both cases, the current waveform was modeled in the forward computations, in order to obtain inversion results not affected by the acquisition settings (Fiandaca et al. 2012). All settings used for inverting the CPA- and Cole-Cole models were identical with the exception of the parameterization.

Since the IP decays had been measured during only 1 second, it was difficult to reliably resolve the spectral parameters τ and c during the inversion. With such short acquisition times, the data were fitted at least equally as good with the CPA model. For this reason, the CPA inversion models will generally be shown in the following, except for one example where both inverted CPA and Cole-Cole models will be shown for comparison. The CPA models will be shown both in terms of the inverted parameters (ρ and ϕ) and of the normalized phase angle $\phi\sigma$, obtained dividing the inverted phase angle ϕ by the inverted resistivity ρ cell by cell. Figure 4 shows qualitative examples of the fit between the data and the inverted CPA model.

Figure 4. Inverted decay curves (red lines) fitted to the data (black lines) during the CPA inversion. Most decays were fitted with the CPA model (left) while some decays contained spectral information neglected in the CPA inversion (right).

4. RESULTS

In section 4.1, we will show results from three of the nine CPA inverted DCIP-lines; two of which were measured directly upon the source zone in the southwestern part of the site (lines A and C in Figure 3 in section 3.1). The third and northernmost line (Line G) is shown as a reference since only small amounts of chlorinated hydrocarbons, situated mainly in the clay layer above the till, were discovered here. In section 4.2, we will also show results from Line A inverted with the Cole-Cole model for a comparison with the CPA results.

4.1. CPA INVERSION RESULTS AND INTERPRETATION

Figure 5 show the CPA inverted results from Line A together with geological reference data. Below the thin fill layer is a low resistive clay layer in the SW half of the profile, extending vertically to -4 mamsl (Figure 5a, upper and lower limits indicated by dotted and dashed lines respectively). The the vertical and horizontal extension of the clay layer is more clearly distinguishable in the phase section (Figure 5b), where it gives rise to an anomaly of low phase. In agreement with the geological reference data, the clay layer becomes thinner from x-distance 30 m and is absent in between x-distances 40-50 m. Also in the NE part of the profile a clay layer is present beneath the fill, but here, it is interspersed with layers of peat and gyttja clay. As the wetland is approached, the layer quickly grows thicker towards the NE from x-distance 50m towards the end of the profile (Figure 5a, dashed line). The layer is characterized by low resistivity (Figure 5a) and high- to intermediate phase (Figure 5b), where the lowest resistivity and highest phase values seem to correspond to presence of peat (dotted lines in Figure 5a-b). A discrimination between organic material and clay is effectively seen in the normalized phase section (Figure 5c), where the layer of high normalized phase correlate well with confirmed peat presence in the reference boreholes.

Figure 5. CPA inverted sections of Line A with superposed geological reference data (a-c). The black dashed line represent the border between the clay layers and the sandy till, while the dotted line show the limits between fill, clay and peat layers. a) The resistivity of the sandy till is generally low with the exception of a high-resistive anomaly (red dashed line). b) The phase angle is generally low with the exception of two anomalies (red dashed lines). c) The center phase anomaly is also visible in the normalized phase angle profile (red dashed line), which indicate that it is not related to variations in groundwater chemistry. d) The chemical reference data show that the zone of highest concentrations of chlorinated hydrocarbons (boreholes 728 and 711, which indicate the PCE source zone) is located in between the phase anomalies.

Below the fill- and clay layers in Figure 5 (the black dashed line in Figure 5a-c), the geophysical data correspond exclusively to sandy chalk till. As can be seen in Figure 5a, the resistivity is generally low with the exception of a high-resistive anomaly (red dashed line). The reference data do not indicate a major geological difference between the higher- and lower resistive zones in the till, but it is possible that these

variations are caused by slight differences in grain size distribution that may have been overlooked during the geological classifications. The phase values in the sandy chalk till (Figure 5b) are generally low as expected for sand and chalk. However, two clearly distinguishable anomalies with high phase values can be seen at x-distances 0 – 10 m and 20 - 35 m respectively (red dashed lines). These anomalies cannot be explained by geological variations in the till material as no e.g. clayey zones have been discovered in the sandy chalk till. Furthermore, the center anomaly is also visible in the normalized phase section (Figure 5c), which indicate that it is not connected to variations in groundwater chemistry.

In Figure 5d, chemical reference data from boreholes along Line A are plotted together with lines representing the geological interpretations from and the phase anomalies in the geophysical data. Just west of the center phase anomaly, the chemical reference data show that the total chlorinated hydrocarbon concentrations are at a maximum, which indicate the location of the PCE source zone (Figure 3 in section 3.1). The location of the source zone (Figure 5d) correspond to high values in resistivity (figure 5a). However, it is uncertain if the source of the observed high resistivity is due to free-phase contamination, coarser till or a combination thereof. The center phase and normalized phase anomaly is located in a zone which is characterized by intermediate concentrations of chlorinated hydrocarbons (Figure 5d). While the concentrations are high at the SW border of the phase anomaly, they are intermediate inside it and are becoming essentially zero beyond the NE border.

The patterns of the phase anomalies in the till in relation to chemical borehole data are consistent in all of the nine measured DCIP profiles. Phase anomalies surrounding high hydrocarbon concentrations in the till are visible in lines A-E. Another example is shown in Figure 6, where the CPA inverted results from Line C are shown. The resistivity, phase and normalized phase distributions in the sandy till show patterns similar to those in Line A (Figure 5), i.e. a high resistive anomaly coinciding with the location of the chlorinated hydrocarbon source zone (Figure 6a, red dashed line) and a phase anomaly NE of the source zone (Figure 6b and 6d, red dashed line) which is also visible in the normalized phase section (Figure 6c). In Line C, a second strong phase anomaly located SW of the source zone is visible in both the phase and the normalized phase sections (Figure 6b-c). Based on the location of this anomaly close to edges of the inverted sections,

it is possible that it is enhanced due to border effects, but a physical cause of these anomalies cannot be ruled out.

Figure 6. *CPA inverted sections of Line C with superposed geological reference data (a-c). The black dashed line represent the border between the clay layers and the sandy till, while the dotted line show the limits between fill, clay and peat layers. a) The resistivity of the sandy till is generally low with the exception of a high-resistive anomaly (red dashed line). b) The phase angle is generally low with the exception of two anomalies (red dashed lines). c) Both phase anomalies are also visible in the normalized phase angle profile (red dashed lines), which indicate that it is not related to variations in groundwater chemistry. d) The chemical reference data show that the zone of highest concentrations of chlorinated hydrocarbons (boreholes 728, 711 and 712, which indicate the PCE source zone) is located in between the phase anomalies.*

In lines F-I, high hydrocarbon concentrations are only found in the upper clay layer, and the IP effects in the till are generally very low. Figure 7 shows an example of data from Line G, where the concentrations are low in the till and there is no longer an apparent phase anomaly visible below the clay layers (Figure 7b-c). The geological stratigraphy is similar to lines A and C according to the geological reference data, although the resistivity values are more heterogeneous compared to in Lines A and C (Figure 7a).

High resistivity in the till where high total chlorinated hydrocarbon concentrations have been measured is visible in many of the profiles, but the resistivity anomalies do not show the same consistency in relation to the chemical data as the phase anomalies. It is probable that the high resistive anomalies are caused by both high concentrations of chlorinated hydrocarbons and/or zones of coarser till material. Gravel and cobbles have been observed locally in a few of the reference boreholes, although the major parts of the sandy chalk till consist mainly of sand-sized grains.

Figure 7. *CPA inverted sections of Line G with superposed geological reference data (a-c). The black dashed line represent the border between the clay layers and the sandy till, while the dotted line show the limits between fill, clay and peat layers. a) The resistivity of the sandy till is*

more heterogeneous compared to Lines A and C. b) The phase angle is low. c) No normalized phase angle anomalies can be distinguished in the till d) The chemical reference data show that high concentrations of chlorinated hydrocarbons are only found in the clay layers. The low values found in the till do not seem to give rise to phase anomalies.

In Figure 8, the CPA inverted resistivity and phase data have been interpolated between the 2D profiles, and the highest values encountered in the sandy chalk till (resistivity above 130 Ωm and phase above 3 mrad) at levels -5 to -14 mamsl have been visualized in a map. When the locations of the high-resistive anomalies in Figure 8 are compared to the distribution of the PCE source zone in Figure 3 (section 3.1) some resemblance can be seen. The Cis-1,2-DE distribution NE of the PCE source zone in Figure 3, which indicate the location of the degradation zone, correlate well with the phase anomalies in Figure 8. The phase anomalies close to the SW border of the investigation area in Figure 8 indicate an additional degradation zone SW of the PCE source zone. Such a widely distributed degradation zone is not indicated by the interpolated Cis-1,2-DE distribution in Figure 3 due to a lack of chemical data between boreholes 728 and 704. However, high concentrations of Cis-1,2-DE have been measured in borehole 728 which is located just SW of the PCE source zone in Figure 3. It is therefore likely that a degradation zone actually exist in the SW part of the site and extends beyond borehole 728, as indicated by the phase anomalies in Figure 8.

Figure 8. Map showing the highest resistivity- and phase values in the sandy till (-4 to -14 mamsl), obtained through interpolation of the resistivity and phase values in the CPA inverted 2D sections.

4.2 COMPARISON WITH COLE-COLE INVERSIONS

In Figure 9, one of the CPA inverted models shown above (Line A) is compared to the Cole-Cole inverted results of the same data. The resistivity pattern in the Cole-Cole inverted model is, as expected, similar to the pattern in the CPA inverted model (Figure 9a). Also the location of the discussed IP anomalies in the till, i.e. high ϕ and m_0 respectively, is similar (red dashed lines in Figure 9b). A difference between the m_0 and the ϕ sections is that the center m_0 anomaly (x-distance 25-40 m) seem to extend throughout the SW half of the Cole-Cole inverted profile, connecting to another high m_0 anomaly located at the SW border of the

investigated line. The SW border anomaly is also visible in the CPA inverted ϕ section; however, it is much weaker compared to the Cole-Cole inverted m_0 section.

In Figure 9 c-d, it can be seen that the discussed m_0 anomaly seem to correspond to areas with relatively low τ and a varying c (Figure 9b-d, red dashed lines). Where m_0 is strongest, the inverted c results are high. These patterns are consistent in all of the nine Cole-Cole inverted profiles. As mentioned in section 3.3, the short acquisition times and noise affected IP decays resulted in an uncertainty in the inverted Cole-Cole parameters τ and c. Even so, the inverted results are good enough to provide a rough estimation of the variation of these parameters at locations where the signal-to-noise ratio is high, i.e. where m_0 is high.

Because of the general uncertainty in the spectral parameters due to the short acquisition range, we constrict our interpretation of the Cole-Cole inverted results to the fact that the discussed m_0 anomalies in the till seem to comprise low τ.

Figure 9. Comparison of Line A inverted with the Cole-Cole model (left) and CPA model (right). The IP anomaly located east of the highest contaminated area is marked with a dashed line, and it can be seen that shorter relaxation times have been measured here compared to the surrounding till.

5. DISCUSSION

The field results presented in section 4 show that high DNAPL concentrations in the soil did not give any measurable IP response, while zones with intermediate DNAPL concentrations gave enhanced IP effects and indicated decreased τ. Considering the spatial location of the ϕ anomalies next to the source zone of free-phase PCE (Figure 5d and 6d in section 4.1) and with support from the chemical data in Figure 3 (section 3.1), we interpret these anomalies as representations of degradation zones in the outer edges of the PCE source zone. In a degradation zone, we believe that the partial degradation and dissolution of a continuous free-phase contamination can be expected to result in residual free-phase DNAPL in the soil pores. However, enhanced ϕ (or m_0) and decreased τ due to NAPL presence is in a general sense contradictory to the results from several other studies, since many of them indicate decreased IP effects (Börner et al. 1993;

Vanhala et al. 1992; Vanhala 1997; Chambers et al. 2004; Martinho et al. 2006; Schmutz et al. 2010; Revil et al. 2011) and often increased τ (Schmutz et al. 2010; Schmutz et al. 2012; Revil et al. 2011; Flores Orozco et al. 2012) in NAPL contaminated compared to clean soil. In order to explain our results, we therefore review some of the conceptual interpretation models that have been used in earlier studies, and complement them by other possible NAPL configurations that have not been discussed previously. The description of the expected IP behavior of these simplified systems will be carried out in terms of Cole-Cole parameters, since these are both effective and commonly used to describe IP spectra in both time- and frequency domain.

5.1 CONCEPTUAL MODELS OF NAPL SATURATED PORE SPACE

If the soil pores are essentially saturated with non-conductive free-phase NAPL, the two scenarios depictured in Figure 10 can be considered. The configuration of NAPL around the soil grains depends on whether the geological material is water-wet or oil-wet. A discussion of the factors that determine the wettability of the interface between geological materials and NAPLs is outside the scope of this paper and can be found elsewhere (Zinszner & Pellerin 2007). Regardless of the wettability, however, full free-phase NAPL saturation in a soil usually makes it impossible to inject current into the sample and measure the IP response in lab (e.g. Schmutz et al. 2010). On the other hand, a zone of NAPL saturated soil could in theory be detectable in field measurements as an anomaly with low m_0 . Low m_0 would be the result of suppressed membrane and/or Stern layer polarization mechanisms due to the displacement of the pore water by the NAPL.

Figure 10. Conceptual models showing the arrangement of NAPL in nearly fully saturated water-wet and oil-wet porous media. In both cases, the IP response can be expected to be absent.

5.2 CONCEPTUAL MODELS OF RESIDUAL NAPL IN WATER SATURATED PORE SPACE

When the soil is not fully saturated with NAPL, there is a variety of possible geometrical arrangements of the free-phase product, and we constrict ourselves here to the case of residual NAPL presence in an otherwise water-saturated pore space. The geometrical configuration of the residual NAPL depend on

455 factors such as the wettability, the capillary pressure and the dynamic history of the NAPL in the pore space
456 (Zinszner & Pellerin 2007). Figure 11 gives four different conceptual models which are possible during
457 different circumstances, and the geometrical configurations in these models could affect measured spectral
458 IP parameters in different ways. In model A, the NAPL is trapped in the soil pores while it in principle also
459 could be trapped in the pore throats (model B), interconnected between several pores (model C) or coating
460 the grain surfaces (model D). In contrast to models C and D, the effects of the conceptual models A and B
461 on IP response or Cole-Cole parameters have not been thoroughly discussed in previous research.

462 *Figure 11. Conceptual models showing possible residual NAPL configurations in a water saturated*
463 *porous media. Each of these configurations can be expected to affect measured IP responses*
464 *in a different way. Model A: the NAPL is distributed as isolated droplets in the pores. Model*
465 *B: the NAPL droplets are trapped in the pore throats. Model C: the NAPL forms a continuous*
466 *phase through several pores. Model D: the NAPL is coating the grains.*

467 *5.2.1 MODEL A*

468 Assuming that the NAPL is present as isolated spheres or blobs in the pores of the granular media (model A
469 in Figure 11), we can expect an increase in m_0. This can be explained by either the electrochemical or the
470 membrane polarization mechanism. It has been shown that a negative surface charge arises at the
471 interfaces between non-polar oil droplets and water, caused by adsorption of hydroxyl ions (Marinova et
472 al. 1996). Analogous to the EDL that forms at grain-water interfaces, the water-oil interfaces will also attract
473 counter ions, leading to the formation of polarizable EDL that can add up to a larger IP response of the soil
474 system. A second contributing factor to increased m_0 in model A would be that a larger portion of the
475 current flows through the EDLs of the grains compared to the conductive preferential pathways made up
476 by free ion mobility in the water, and thus produce enhanced polarization, a process that has been
477 described by Titov et al. (2004) for unsaturated sands. According to the electrochemical polarization
478 mechanism, the Cole-Cole peak relaxation time τ is proportional to the dominant radius of the (assumed
479 spherical) particles (Lesmes & Frye 2001; Revil & Florsch 2010). With the presence of NAPL droplets in the
480 pores (which are smaller than the dominant grain size), it can be assumed that the dominant size of the

spheres (grains and NAPL droplets) decrease, resulting in a decreased τ in the soil volume. Because of the greater range of particle sizes and relaxation times τ, the frequency factor c can also expected to decrease. Although these effects may be likely for many natural materials with a relatively broad particle size distribution, a second peak in the frequency spectra may be more likely to appear in a very well sorted medium.

In terms of the membrane polarization mechanism, the space between the grains and the NAPL droplets can be considered as the ion selective (narrow) zone while the pore throats makes up the non-selective (wide) zones, i.e. the opposite to the situation in clean granular material where the pore throats make up the selective zones and the non-selective zones are constituted by the pores (Titov et al. 2002; Titov et al. 2004). Compared to a clean sample, $m_0$would increase with NAPL presence since the variation ion transparency between the zones becomes larger (Titov et al. 2004). Since τ is determined by the length of the non-selective zones (Vinegar & Waxman 1984; Titov et al. 2002) and the pore throats (i.e. grain contacts) have smaller length scales than the pores, τ can be expected to decrease in NAPL contaminated soil. The frequency factor c is dependent on the distribution of non-selective zone lengths. Thus, the presence of NAPL droplets in a portion of, but not all, pores would possibly increase the dispersion of relaxation times τ.

NAPL droplets in soil pores was proposed but not discussed by Martinho et al. (2006).The NAPL configuration in model A is also similar to the conceptual model of air-filled pores in water saturated soil studied by Titov et al. (2004), who interpreted a measured increased m_0 in NAPL contaminated samples as a result of mechanisms identical to increased m_0 of unsaturated samples. However, the NAPL configuration in model A does not require that entire pore spaces are filled with NAPL, and the mechanism of NAPL displacement over water is not the same as water drainage of pores in a soil.

5.2.2 MODEL B

If the residual NAPL is assumed to be trapped in the pore throats (model B in Figure 11) instead of in the pores, the electrochemical polarization mechanism would still be expected to work identically as in case A, i.e. increased m_0, decreased τ and decreased c. However, the membrane polarization mechanism would

differ in this case, since the non-selective zones appears in the pore throats for both clean and contaminated samples. The chargeability m_0 would still increase by NAPL droplets due to the decreased ion transparency in the narrower pore throats, but the lengths of the non-selective zones, and consequently τ and c, would probably remain unchanged.

5.2.3 MODEL C

In model C (Figure 11), it is assumed that the free-phase NAPL is interconnected between several pores and pore throats. It can be expected that part of the electrochemical polarization present in a clean sample would be short-circuited by surface conduction along the EDLs of the interconnected residual NAPL, similarly to what have been observed for clays where the microstructure results in a conductive continuum rather than unconnected and polarizable EDLs or series of alternating ion transparency (Marshall & Madden 1959). In addition, membrane polarization effects would vanish since this mechanism require diffusion of mobile ions in the pore fluid. The net polarization m_0 is therefore expected to decrease with NAPL presence, until the soil eventually approaches the fully NAPL-saturated case (Figure 11) and results in a flat IP spectrum. This means that c is expected to decrease while τ is left unchanged. We believe that in the case of a NAPL configuration according to model C, the decrease in polarization magnitude would be related to an interconnected EDL of the NAPL rather than a suppression of the EDLs forming around the mineral grains.

Conceptual models similar to Figure model C (Figure 11) have been published by Schmutz et al. (2010) and Revil et al. (2011) for the water-wet distribution of LNAPLs in the pore space. In addition, they also presented a variant on model C where the geological material is assumed to be oil-wet rather that water-wet. This condition results in a full or partial prohibition of the EDLs around the affected grains in contact with the interconnected EDL, and this conceptual model have also been presented by Flores Orozco et al. (2012).

In contradiction to our qualitative predictions above, Schmutz et al. (2010; 2012) saw an increase in σ'' with increasing LNAPL content during water-wet conditions, a result which was attributed to the decrease in water saturation. In contrast, decreased σ'' were measured by Revil et al. (2011) for oil-wet conditions as well as decreased m_0 by Flores Orozco et al. (2012) in a field study of a LNAPL spill. Revil et al. (2011)

interpreted the decrease in σ'' to depend on an increased cation exchange capacity (CEC) at the oil-water interface due to presence of polar molecules in the NAPL, resulting in increased surface conduction and a disappearance of polarization length scales, while Flores Orozco et al. (2012) interpreted their observation as a result of prevented of EDL formation. In most cases, increased τ were observed in these studies (Schmutz et al. 2010; Schmutz et al. 2012; Revil et al. 2011; Flores Orozco et al. 2012), but these observations were not interpreted as a result of the NAPL configuration in model C. Therefore, these studies are not in contradiction to our expectation of unchanged τ due to the NAPL configuration in model C. The observed effects on τ may instead be related to other superposed mechanisms, e.g. Maxwell-Wagner effects (Revil et al. 2011) or mixed NAPL configurations (Flores Orozco et al. 2012).

5.2.4 MODEL D

In model D (Figure 11), it is assumed that the NAPL coats grain surfaces and thereby prohibits grain EDL formation. Martinho et al. (2006) interpreted their data in terms of model D, where organic molecules coating clay particles would explain the observed decrease in m_0 in the range 10-20% gasoline concentration in a sandy loam. Prior to Martinho et al. (2006), Olhoeft (1985) suggested a similar process whereby organic molecules attach to the clay surfaces and inhibit the cation exchange processes, given that the actual organic molecules are soluble in water. Nevertheless, Olhoeft (1985) showed that the net effect of organic contaminants on the measured ϕ was an increase, induced by unspecified chemical effects, so called clay-organic reactions.

Focusing only on the effects of the NAPL configuration, it is reasonable that a decreased m_0 can be observed for clay grains, given that their assumable high CEC would lead to a considerable stronger EDL if NAPLs are absent. On the other hand, the effect of NAPL coating on e.g. sand grains may be much more subtle and the response of m_0 is difficult to judge since it depends on the relative strength of the NAPL and grain EDLs. In terms of the electrochemical polarization mechanism, τ is expected to increase since the dominant diameters of the polarizing spheres (grain and NAPL) will increase. Assuming that not all grains are coated by NAPL, the frequency factor c could be expected to decrease.

In terms of the membrane polarization effect, it can be argued that the generally narrower zones will have a greater effect on ion transparency in the pore-throats compared to the pores, which will still mainly consist of pore fluid. Thus, the contribution of the membrane mechanism to the net polarization m_0 may be an increase. In addition, decreased τ can be expected according to the membrane mechanism since the length scale of the pores will be reduced by the NAPLs. Assuming again that not all grains are coated by NAPL, the distribution of pore lengths will increase resulting in a broader relaxation spectra and decreased c.

5.2.5 SUMMARY

The conceptual models in Figure 11 and the discussion above covers a wide range of possible NAPL configurations in the pore space, each expected to affect the spectral IP parameters in different ways (summarized in Table 1). However, in a real sample or field site, it is not obvious that all parts of the residual NAPL are arranged in a certain way: a combination of one or several of the conceptual models in Figure 11 is probably possible.

Table 1. Summarizing table showing the expected effects of the different NAPL distributions in Figure 12 on the electrochemical- and membrane polarization mechanisms in terms of Cole-Cole parameters.

Conceptual model	**Chargeabiliy (m0)**		**Relaxation time (τ)**		**Frequency factor (c)**	
	Electro-chemical	**Membrane**	**Electro-chemical**	**Membrane**	**Electro-chemical**	**Membrane**
A	Increase	Increase	Decrease	Decrease	Decrease	Decrease
B	Increase	Increase	Decrease	Unchanged	Decrease	Unchanged
C	Decrease	Not present	Unchanged	Not present	Decrease	Not present

D	Decrease or increase	Increase	Increase	Decrease	Decrease	Decrease

574

575 Although outside the scope of this paper, it is worth mentioning that a variety of NAPL configurations could
576 be possible also in unsaturated material where air constitutes a third phase in the pore system together
577 with NAPL and water. For example, Shefer et al. (2013) presented a conceptual model of these conditions,
578 where the NAPL was, as we understand it, assumed to create rings around air-filled pores by displacement
579 of the water phase.

580 ***5.3 INTERPRETATION OF FIELD DATA***

581 In our field data, the source zone of free-phase PCE did not give rise to any ϕ anomalies. The chemical
582 sampling results showed high concentrations of chlorinated hydrocarbons, and it is probable that the
583 DNAPL to a large degree forms a continuous and interconnected phase in the pore space at this location
584 (model C above).

585 Several decades have passed since the release of the contaminant and parts of the PCE has degraded and
586 dissolved into the ground water. Around the borders of the continuous PCE source zone, microorganisms
587 get access to the contaminant and use it as a carbon source. We believe that the biodegradation may
588 fractionate the continuous PCE leading to a distribution more similar to model A above, i.e. isolated droplets
589 in the soil pores. We have shown that the expected behavior of NAPL arranged in this way is an increase of
590 m_0 (or ϕ), in terms of both electrochemical and membrane polarization mechanisms. This means that the
591 enhanced IP effects that were observed outside the source zone in our field data (Figures 5b-d, 6b-d and 8)
592 probably represent a degradation zone. This interpretation is supported by the spatial pattern of the
593 chemical sampling results in Figure 3 (section 3.1) and Figures 5 and 6 (section 4.1), going from high
594 concentrations to low with the main ϕ anomaly coinciding with medium concentration of chlorinated
595 hydrocarbons. Furthermore, the Cole-Cole inversions of our field data (Figure 8) indicated lower τ and
596 higher c corresponding to the same ϕ anomalies. The inverted τ models also supports the expected

behavior of model A, although the results from the Cole-Cole inversion should be interpreted with some caution.

It should be pointed out that even though the geometrical arrangement of NAPLs in the pores is an important parameter controlling the IP response, there are also other contributing factors that could explain enhanced IP effects in a degradation zone. For example, it has been shown that microbial growth in hydrocarbon contaminated soil leads to increased IP effects, probably due to pore constriction or attachment of microbial cells around grains (Abdel Aal et al. 2006; Atekwana & Slater 2009). Some bacterial activity can also involve iron precipitation (Atekwana & Slater 2009) or create favorable conditions for iron sulfate precipitation by inducing groundwater chemistry changes (Flores Orozco et al. 2011). Since microbiological and groundwater chemical factors were outside the scope of this investigation, it is unknown if such effects could be possible at this specific site. Future research is needed in order to enable a discrimination between IP effects induced by the NAPL itself and possible effects of microbiological activities in a degradation zone.

The comparison between the horizontally interpolated ϕ anomalies in Figure 8 (section 4.1) and the interpolated chemical reference data in Figure 3 (section 3.1) show an overall good agreement of the ϕ anomalies and the degradation zone (as indicated by the Cis-1,2-DE distribution). A perfect correlation cannot be expected since the drilling data do not show an absolute extension of the contaminants; in order to achieve this, the sampling would need to be even denser and cover the full length of every borehole. An interesting example is the ϕ anomaly encountered close to the SW border of the investigated site; although one borehole (728 in Figure 3, section 3.1) indicate a degradation zone going from the source zone in this direction, its extension cannot be determined due to a lack of chemical data. In addition, the scale differences between DCIP data and chemical data as well as the fact that the interpretation of the ϕ anomalies as degradation zones are based on the total amount of free-phase product in the pore space and not the NAPL species (visualized in Figure 3), some deviations between the patterns in Figure 3 and Figure 8 are unavoidable.

Our inverted c models contradicts our expectation of decreased c for all the discussed residual NAPL configurations. However, it is possible that the apparently high c may merely be an effect of a zone of high m_0 surrounded by natural till material with a broad τ distribution. More research is needed to investigate the IP spectra in natural soils and the relationships between lab results and the inverted spectral parameters measured in field. For field data, the possibility of choosing either the Cole-Cole or the CPA model provides a valuable flexibility in the inversion process that may be important in overcoming these scale differences.

Future research is needed to verify the expected spectral IP responses of different conceptual models (Figure 12 and Table 1), as well as to investigate the effects of possible Maxwell-Wagner mechanisms on measurement data from NAPL contaminated soil. In order to further improve the applicability of the method in environmental projects, more research is also needed on the technical issues associated with field measurements. Full-waveform measurements in time domain are robust and time efficient, but further development is necessary in order to achieve data from the earliest times after the current switch off and cover a spectral range comparable to frequency domain measurements. However, since the IP mechanisms we are interested in usually occur at relatively low frequencies, the long acquisition times necessary for the collection of spectral IP data is probably a more challenging problem in both time- and frequency domain field measurements.

6. CONCLUSIONS

The potential of detecting NAPL with frequency- or time domain IP has been investigated in a number of lab and field studies, but the results in these studies are inconsistent and sometimes even contradictory. Different conceptual models have been proposed to explain the results from individual authors, and an overall understanding of the effects of NAPL on the porous system has not yet been achieved. In this study, we review and discuss around possible conceptual models (section 5) and conclude that the spatial configuration of residual NAPLs in a water-saturated pore space may influence the IP mechanisms in different ways. While a decrease in chargeability or phase can be expected for some configurations, the opposite may be true for others. The NAPL configurations in different samples or field sites are often

unknown, and this may to some extent explain why different results have been achieved by different authors.

In our field case, we believe that the DNAPL forms a more or less continuous phase in the pore space of the source zone leading to an absence of IP effects. The observed increase in phase and normalized phase angle next to the source zone is interpreted as a degradation zone. It is suggested that the ongoing biodegradation may have led to a fractionation of the continuous DNAPL in the outer part of the original source zone, leading to a residual presence of isolated DNAPL droplets in the soil pores. Another contributing factor to the increased IP effects may be the presence of microbial cells in the degradation zone or microbial induced changes in the geochemical environment.

In summary, an understanding of the influence of free-phase NAPLs on spectral IP parameters makes the method a promising tool to improve field delineation of NAPL contaminants in the ground. Furthermore, the ability to detect degradation zones enables monitoring of the natural biodegradation or stimulated in-situ degradation of NAPL spills.

ACKNOWLEDGEMENTS

We would like to thank the two anonymous reviewers who helped to improve the quality and clarity of the paper. We also thank our project colleagues and field co-workers Per-Ivar Olsson, Marcus Wennermark, Carl-Henrik Månsson and Mikael Lumetzberger, as well as the PhD students at Engineering Geology, Lund University Patrik Fröjd, Kristofer Hellman and Oskar Baggens. Funding for the work was provided by Formas - The Swedish Research Council for Environment, Agricultural Sciences and Spatial Planning, (ref. 2012-1931), BeFo - Swedish Rock Engineering Research Foundation, (ref. 331), SBUF - The Development Fund of the Swedish Construction Industry, (ref. 12719) and Sven Tyréns Stiftelse. The project is part of the Geoinfra-TRUST framework (http://trust-geoinfra.se/).

REFERENCES

Abdel Aal, G.Z., Slater, L.D. & Atekwana, E.A., 2006. Induced-polarization measurements on unconsolidated sediments from a site of active hydrocarbon biodegradation. *Geophysics*, 71(2), pp.H13–H24. Available at: http://library.seg.org/doi/abs/10.1190/1.2187760.

Ajo-Franklin, J.B., Geller, J.T. & Harris, J.M., 2006. A survey of the geophysical properties of chlorinated DNAPLs. *Journal of Applied Geophysics*, 59(3), pp.177–189. Available at: http://linkinghub.elsevier.com/retrieve/pii/S0926985105000868 [Accessed January 8, 2014].

Atekwana, E.A. & Atekwana, E.A., 2010. Geophysical Signatures of Microbial Activity at Hydrocarbon Contaminated Sites: A Review. *Surveys in Geophysics*, 31(2), pp.247–283. Available at: http://link.springer.com/10.1007/s10712-009-9089-8 [Accessed April 28, 2014].

Atekwana, E.A. & Slater, L.D., 2009. Biogeophysics: A new frontier in Earth science research. *Reviews of Geophysics*, 47(4), pp.1–30. Available at: http://www.agu.org/pubs/crossref/2009/2009RG000285.shtml [Accessed July 1, 2013].

Auken, E. et al., 2014. An overview of a highly versatile forward and stable inverse algorithm for airborne, ground-based and borehole electromagnetic and electric data. *Exploration Geophysics*, pp.1–13. Available at: http://dx.doi.org/10.1071/EG13097.

Binley, A. et al., 2005. Relationship between spectral induced polarization and hydraulic properties of saturated and unsaturated sandstone. *Water Resources Research*, 41(12), p.n/a–n/a. Available at: http://doi.wiley.com/10.1029/2005WR004202 [Accessed August 30, 2013].

Börner, F., Gruhne, M. & Schön, J., 1993. Contamination indications derived from electrical properties in the low frequency range. *Geophysical Prospecting*, 41(1), pp.83–98.

Cassiani, G. et al., 2009. Spectral induced polarization for the characterization of free-phase hydrocarbon contamination of sediments with low clay content. *Near Surface Geophysics*, 7(5-6), pp.547–562.

Chambers, J.E. et al., 2004. Non-invasive monitoring of DNAPL migration through a saturated porous medium using electrical impedance tomography. *Journal of contaminant hydrology*, 68, pp.1–22.

694 Cole, K.S. & Cole, R.H., 1941. Dispersion and Absorption in Dielectrics I. Alternating Current Characteristics. *The*
695 *Journal of Chemical Physics*, 9(4), p.341. Available at:
696 http://scitation.aip.org/content/aip/journal/jcp/9/4/10.1063/1.1750906 [Accessed March 22, 2014].

697 Dahlin, T., 2000. Electrode charge-up effects in DC resistivity data acquisition using multi electrode arrays.
698 *Geophysical Prospecting*, 48(1), pp.181–187.

699 Dahlin, T. & Leroux, V., 2012. Improvement in time-domain induced polarization data quality with multi-
700 electrode systems by separating current and potential cables. *Near Surface Geophysics*, pp.545–565.
701 Available at: http://nsg.eage.org/publication/publicationdetails/?publication=65633 [Accessed December
702 3, 2013].

703 Dahlin, T., Leroux, V. & Nissen, J., 2002. Measuring Techniques in Induced Polarisation Imaging. *Journal of*
704 *Applied Geophysics*, 50(3), pp.279–298.

705 Deceuster, J. & Kaufmann, O., 2012. Improving the delineation of hydrocarbon-impacted soils and water
706 through induced polarization (IP) tomographies: a field study at an industrial waste land. *Journal of*
707 *contaminant hydrology*, 136-137(August 2012), pp.25–42. Available at:
708 http://www.ncbi.nlm.nih.gov/pubmed/22659399 [Accessed August 5, 2013].

709 Fiandaca, G. et al., 2013. Resolving spectral information from time domain induced polarization data through 2-
710 D inversion. *Geophysical Journal International*, 192(2), pp.631–646. Available at:
711 http://gji.oxfordjournals.org/cgi/doi/10.1093/gji/ggs060 [Accessed August 5, 2013].

712 Fiandaca, G. et al., 2012. Time-domain-induced polarization: Full-decay forward modeling and 1D laterally
713 constrained inversion of Cole-Cole parameters. *Geophysics*, 77(3), pp.E213–E225. Available at:
714 http://library.seg.org/doi/abs/10.1190/geo2011-0217.1.

715 Flores Orozco, A. et al., 2012. Delineation of subsurface hydrocarbon contamination at a former hydrogenation
716 plant using spectral induced polarization imaging. *Journal of contaminant hydrology*, 136-137, pp.131–44.
717 Available at: http://www.ncbi.nlm.nih.gov/pubmed/22784635 [Accessed May 13, 2014].

718 Flores Orozco, A. et al., 2011. Using complex resistivity imaging to infer biogeochemical processes associated
719 with bioremediation of an uranium-contaminated aquifer. *Journal of Geophysical Research:*
720 *Biogeosciences*, 116(3), pp.1–17.

721 LaBrecque, D. & Daily, W., 2008. Assessment of measurement errors for galvanic-resistivity electrodes of
722 different composition. *Geophysics*, 73(2), pp.F55–F64.

723 Leroy, P. et al., 2008. Complex conductivity of water-saturated packs of glass beads. *Journal of colloid and*
724 *interface science*, 321(1), pp.103–17. Available at: http://www.ncbi.nlm.nih.gov/pubmed/18272167
725 [Accessed May 29, 2013].

726 Leroy, P. & Revil, A., 2009. A mechanistic model for the spectral induced polarization of clay materials. *Journal*
727 *of Geophysical Research: Solid Earth*, 114(B10).

728 Lesmes, D.P. & Frye, K.M., 2001. Influence of pore fluid chemistry on the complex conductivity and induced
729 polarization responses of Berea sandstone. *Journal of Geophysical Research*, 106(B3), pp.4079–4090.

730 Lesmes, D.P. & Morgan, F.D., 2001. Dielectric spectroscopy of sedimentary rocks. *Journal of Geophysical*
731 *Research*, 106(B7), pp.13329–13346.

732 De Lima, O.A.L. & Sharma, M.M., 1992. A generalized Maxwell-Wagner theory for membrane polarization in
733 shaly sands. *Geophysics*, 57(3), pp.431–440. Available at:
734 http://library.seg.org/doi/abs/10.1190/1.1443257.

735 Marinova, K.G. et al., 1996. Charging of Oil - Water Interfaces Due to Spontaneous Adsorption of Hydroxyl Ions.
736 *Langmuir*, 12(8), pp.2045–2051.

737 Marshall, D.J. & Madden, T.R., 1959. Induced polarization, a study of its causes. *Geophysics*, XXIV(4), pp.790–
738 816.

739 Martinho, E., Almeida, F. & Senos Matias, M.J., 2006. An experimental study of organic pollutant effects on
740 time domain induced polarization measurements. *Journal of Applied Geophysics*, 60(1), pp.27–40.

741 Available at: http://linkinghub.elsevier.com/retrieve/pii/S092698510500100X [Accessed November 14,
742 2014].

743 Naudet, V. et al., 2014. 3D electrical resistivity tomography to locate DNAPL contamination around a housing
744 estate. *Near Surface Geophysics*, 12(3), pp.351–360. Available at:
745 http://nsg.eage.org/publication/publicationdetails/?publication=75347 [Accessed November 14, 2014].

746 Nordsiek, S. & Weller, A., 2008. A new approach to fitting induced-polarization spectra. *Geophysics*, 73(6),
747 pp.F235–F245. Available at: http://library.seg.org/doi/abs/10.1190/1.2987412.

748 Olhoeft, G.R., 1985. Low frequency electrical properties. *Geophysics*, 50(12), pp.2492–2503. Available at:
749 http://library.seg.org/doi/abs/10.1190/1.1441880.

750 Pelton, W.H. et al., 1978. Mineral discrimination and removal of inductive coupling with multifrequency IP.
751 *Geophysics*, 43(3), pp.588–609.

752 Power, C. et al., 2015. Improved time-lapse electrical resistivity tomography monitoring of dense non-aqueous
753 phase liquids with surface-to-horizontal borehole arrays. *Journal of Applied Geophysics*, 112(January
754 2015), pp.1–13. Available at: http://linkinghub.elsevier.com/retrieve/pii/S0926985114003164.

755 Revil, A. & Florsch, N., 2010. Determination of permeability from spectral induced polarization in granular
756 media. *Geophysical Journal International*, pp.1480–1498. Available at:
757 http://gji.oxfordjournals.org/cgi/doi/10.1111/j.1365-246X.2010.04573.x [Accessed March 15, 2013].

758 Revil, A., Schmutz, M. & Batzle, M.L., 2011. Influence of oil wettability upon spectral induced polarization of oil-
759 bearing sands. *Geophysics*, 76(5), pp.A31–A36. Available at:
760 http://library.seg.org/doi/abs/10.1190/geo2011-0006.1.

761 Schmutz, M. et al., 2010. Influence of oil saturation upon spectral induced polarization of oil-bearing sands.
762 *Geophysical Journal International*, 183(1), pp.211–224. Available at:
763 http://gji.oxfordjournals.org/cgi/doi/10.1111/j.1365-246X.2010.04751.x [Accessed April 28, 2014].

764 Schmutz, M., Blondel, A. & Revil, A., 2012. Saturation dependence of the quadrature conductivity of oil-bearing
765 sands. *Geophysical Research Letters*, 39(3). Available at: http://doi.wiley.com/10.1029/2011GL050474
766 [Accessed June 11, 2013].

767 Schwarz, G., 1962. A theory of the low-frequency dielectric dispersion of colloidal particles in electrolyte
768 solution. *Journal of Physical Chemistry*, 66(12), pp.2636–2642.

769 Scott, J.B.T. & Barker, R.D., 2003. Determining pore-throat size in Permo-Triassic sandstones from low-
770 frequency electrical spectroscopy. *Geophysical Research Letters*, 30(9). Available at:
771 http://doi.wiley.com/10.1029/2003GL016951 [Accessed June 11, 2013].

772 Seigel, H.O., 1959. Mathematical formulation and type curves for induced polarization. *Geophysics*, XXIV(3),
773 pp.547–565.

774 Shefer, I., Schwartz, N. & Furman, A., 2013. The effect of free-phase NAPL on the spectral induced polarization
775 signature of variably saturated soil. *Water Resources Research*, 49(10), pp.6229–6237. Available at:
776 http://doi.wiley.com/10.1002/wrcr.20502 [Accessed October 7, 2013].

777 Slater, L., 2002. Electrical-hydraulic relationships observed for unconsolidated sediments. *Water Resources*
778 *Research*, 38(10), pp.1–13. Available at: http://www.agu.org/pubs/crossref/2002/2001WR001075.shtml.

779 Slater, L., 2007. Near Surface Electrical Characterization of Hydraulic Conductivity: From Petrophysical
780 Properties to Aquifer Geometries—A Review. *Surveys in Geophysics*, 28(2-3), pp.169–197. Available at:
781 http://link.springer.com/10.1007/s10712-007-9022-y [Accessed May 2, 2013].

782 Slater, L. & Lesmes, D.P., 2002. Electrical-hydraulic relationships observed for unconsolidated sediments. *Water*
783 *Resources Research*, 38(10), pp.1–13. Available at:
784 http://www.agu.org/pubs/crossref/2002/2001WR001075.shtml.

785 Slater, L.D. & Lesmes, D., 2002. IP interpretation in environmental investigations. *Geophysics*, 67(1), pp.77–88.
786 Available at: http://link.aip.org/link/GPYSA7/v67/i1/p77/s1&Agg=doi.

787 Titov, K. et al., 2004. Induced Polarization of Unsaturated Sands Determined through Time Domain
788 Measurements. *Vadose Zone Journal*, 3(4), pp.1160–1168.

789 Titov, K. et al., 2010. Relationships between induced polarization relaxation time and hydraulic properties of
790 sandstone. *Geophysical Journal International*, 180(3), pp.1095–1106. Available at:
791 http://gji.oxfordjournals.org/cgi/doi/10.1111/j.1365-246X.2009.04465.x [Accessed June 14, 2013].

792 Titov, K. et al., 2002. Theoretical and experimental study of time domain-induced polarization in water-
793 saturated sands. *Journal of Applied Geophysics*, 50(4), pp.417–433.

794 Vanhala, H., 1997. Mapping oil-contaminated sand and till with the spectral induced polarization (SIP) method.
795 *Geophysical Prospecting*, 45(2), pp.303–326.

796 Vanhala, H., Soininen, H. & Kukkonen, I., 1992. Detecting organic chemical contaminants by spectral induced
797 polarization method in glacial till environment. *Geophysics*, 57(8), pp.1014–1017. Available at:
798 http://library.seg.org/doi/abs/10.1190/1.1443312.

799 Vinegar, H.J. & Waxman, M.H., 1984. Induced polarization of shaly sands. *Geophysics*, 49(8), pp.1267–1287.
800 Available at: http://library.seg.org/doi/abs/10.1190/1.1441755.

801 Van Voorhis, G.D., Nelson, P.H. & Drake, T.L., 1973. Complex resistivity spectra of porphyry copper
802 mineralization. *Geophysics*, 38(1), pp.49–60.

803 Zinszner, B. & Pellerin, F.M., 2007. *A Geoscientist's Guide to Petrophysics*, Paris: Editions Technip.

804

805

FIGURE CAPTIONS

Figure 1. *Satellite image of the investigated site with the positions of the DCIP electrodes. The yellow and red markers represents previously drilled boreholes with geological classifications and chemical sampling data respectively.*

Figure 2. *Principal geological profile across the site, based on geological classifications from the boreholes in Figure 1. The estimated extension of the free-phase contamination is also shown*

Figure 3. *Summarizing results from the chemical analyses of soil samples taken in the sandy chalk till (below -4 mamsl). The interpolated PCE surface show approximately the main location of the source contamination, while the interpolated Cis-1,2-DE surface indicate the main degradation zone.*

Figure 4. *Inverted decay curves (red lines) fitted to the data (black lines) during the CPA inversion. Most decays were fitted with the CPA model (left) while some decays contained spectral information neglected in the CPA inversion (right).*

Figure 5. *CPA inverted sections of Line A with superposed geological reference data (a-c). The black dashed line represent the border between the clay layers and the sandy till, while the dotted line show the limits between fill, clay and peat layers. a) The resistivity of the sandy till is generally low with the exception of a high-resistive anomaly (red dashed line). b) The phase angle is generally low with the exception of two anomalies (red dashed lines). c) The center phase anomaly is also visible in the normalized phase angle profile (red dashed line), which indicate that it is not related to variations in groundwater chemistry. d) The chemical reference data show that the zone of highest concentrations of chlorinated hydrocarbons (boreholes 728 and 711, which indicate the PCE source zone) is located in between the phase anomalies.*

Figure 6. *CPA inverted sections of Line C with superposed geological reference data (a-c). The black dashed line represent the border between the clay layers and the sandy till, while the*

dotted line show the limits between fill, clay and peat layers. a) The resistivity of the sandy till is generally low with the exception of a high-resistive anomaly (red dashed line). b) The phase angle is generally low with the exception of two anomalies (red dashed lines). c) Both phase anomalies are also visible in the normalized phase angle profile (red dashed lines), which indicate that it is not related to variations in groundwater chemistry. d) The chemical reference data show that the zone of highest concentrations of chlorinated hydrocarbons (boreholes 728, 711 and 712, which indicate the PCE source zone) is located in between the phase anomalies.

Figure 7. *CPA inverted sections of Line G with superposed geological reference data (a-c). The black dashed line represent the border between the clay layers and the sandy till, while the dotted line show the limits between fill, clay and peat layers. a) The resistivity of the sandy till is more heterogeneous compared to Lines A and C. b) The phase angle is low. c) No normalized phase angle anomalies can be distinguished in the till d) The chemical reference data show that high concentrations of chlorinated hydrocarbons are only found in the clay layers. The low values found in the till do not seem to give rise to phase anomalies.*

Figure 8. *Map showing the highest resistivity- and phase values in the sandy till (-4 to -14 mamsl), obtained through interpolation of the resistivity and phase values in the CPA inverted 2D sections.*

Figure 9. *Comparison of Line A inverted with the Cole-Cole model (left) and CPA model (right). The IP anomaly located east of the highest contaminated area is marked with a dashed line, and it can be seen that shorter relaxation times have been measured here compared to the surrounding till.*

Figure 10. *Conceptual models showing the arrangement of NAPL in nearly fully saturated water-wet and oil-wet porous media. In both cases, the IP response can be expected to be absent.*

Figure 11. *Conceptual models showing possible residual NAPL configurations in a water saturated porous media. Each of these configurations can be expected to affect measured IP responses in a different way. Model A: the NAPL is distributed as isolated droplets in the*

pores. Model B: the NAPL droplets are trapped in the pore throats. Model C: the NAPL forms a continuous phase through several pores. Model D: the NAPL is coating the grains.

863 **FIGURE 1**

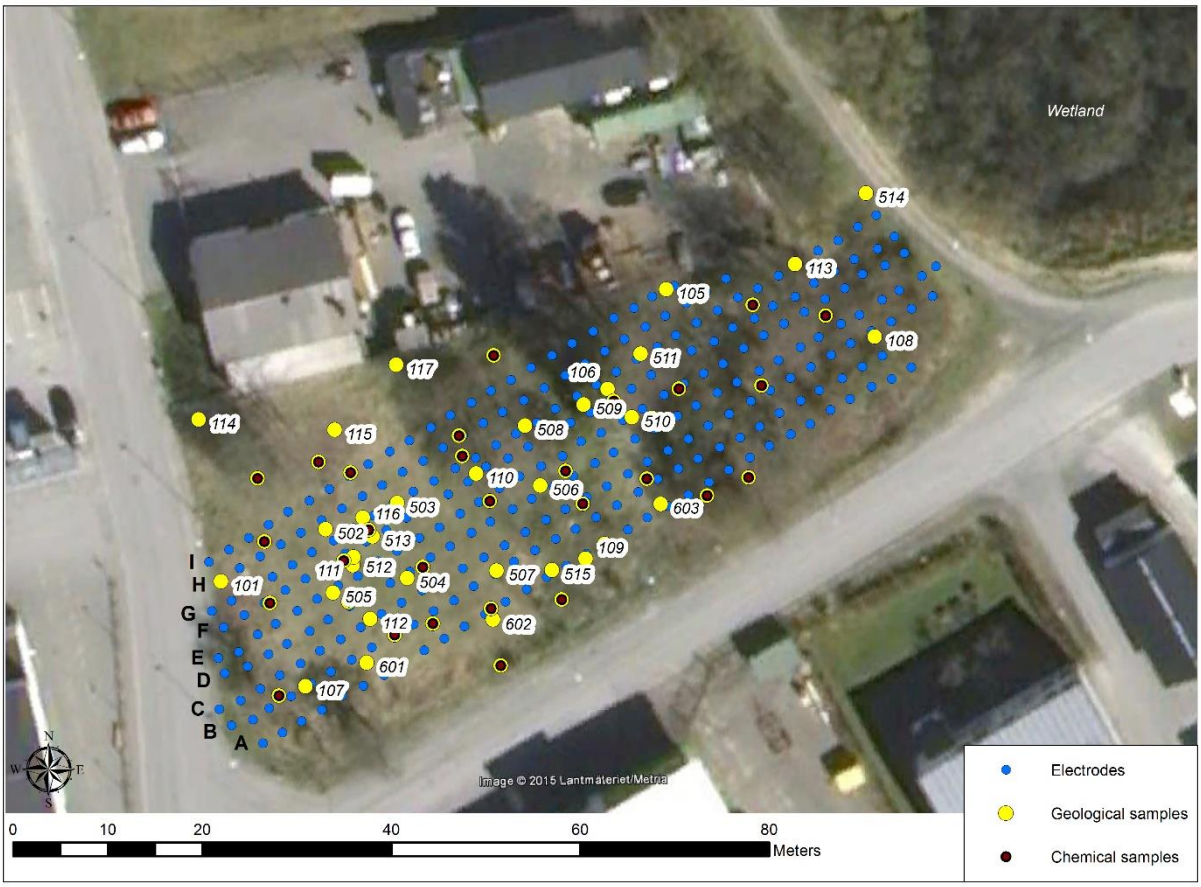

864

865

866 **FIGURE 2**

867

868

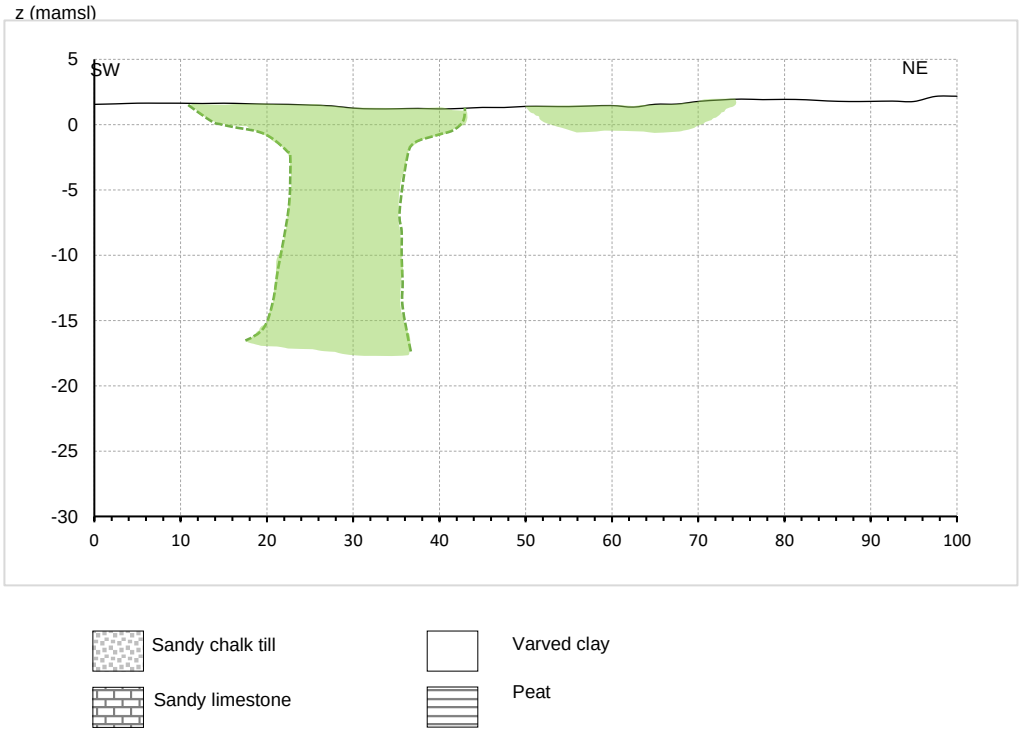

869 **FIGURE 3**

870

871

872 **FIGURE 4**

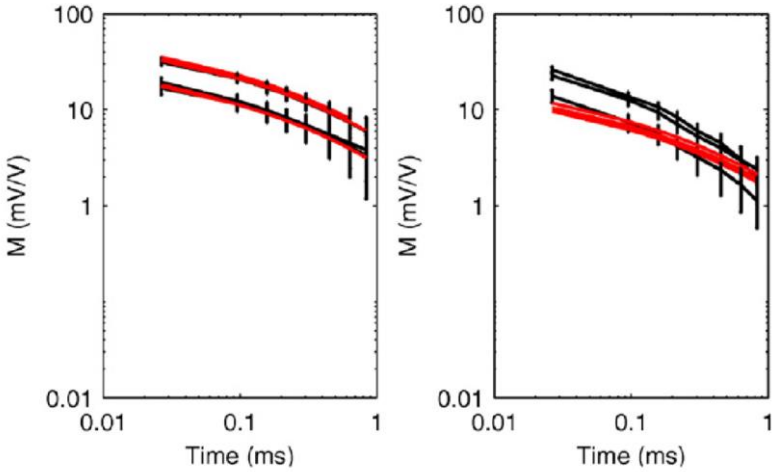

873

874

875 **FIGURE 5**

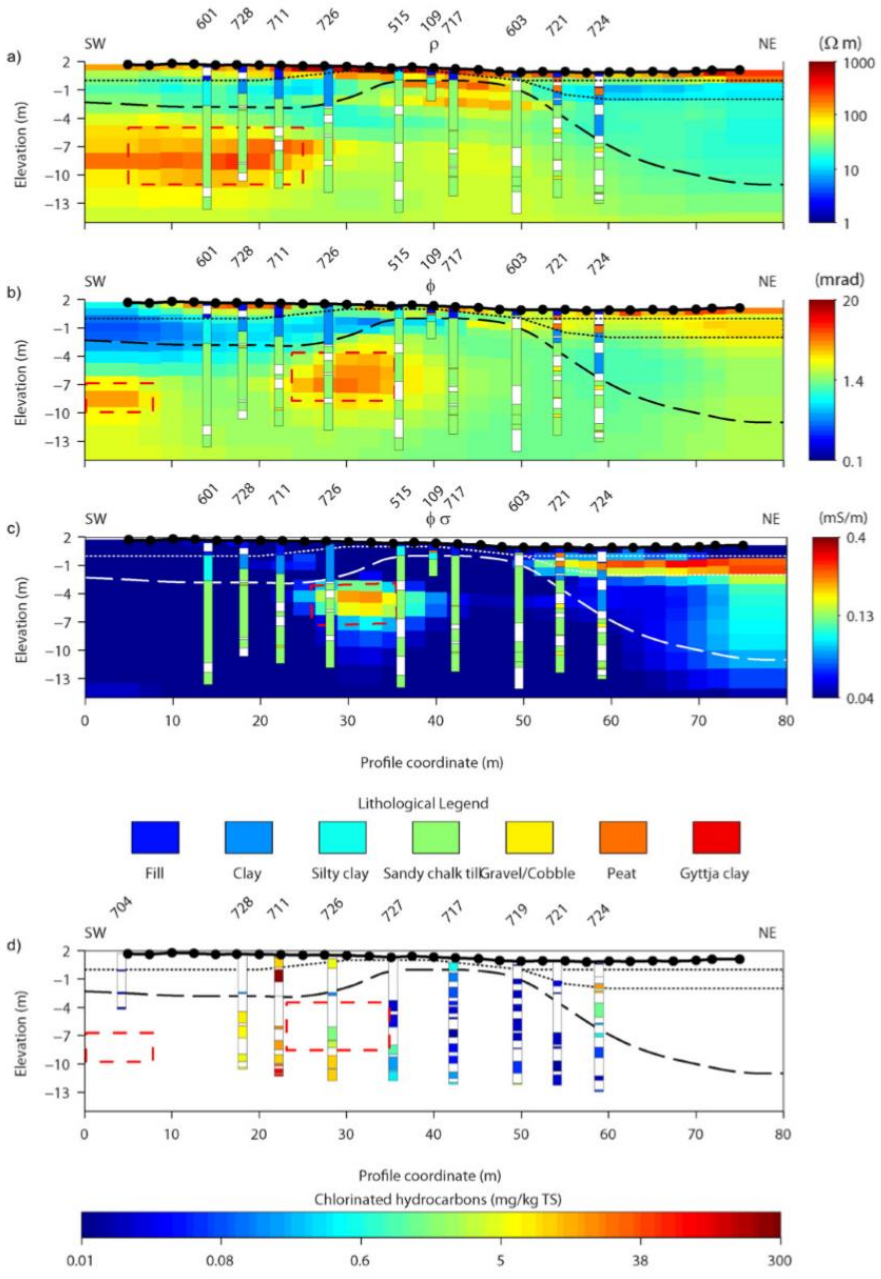

876

877

878 **FIGURE 6**

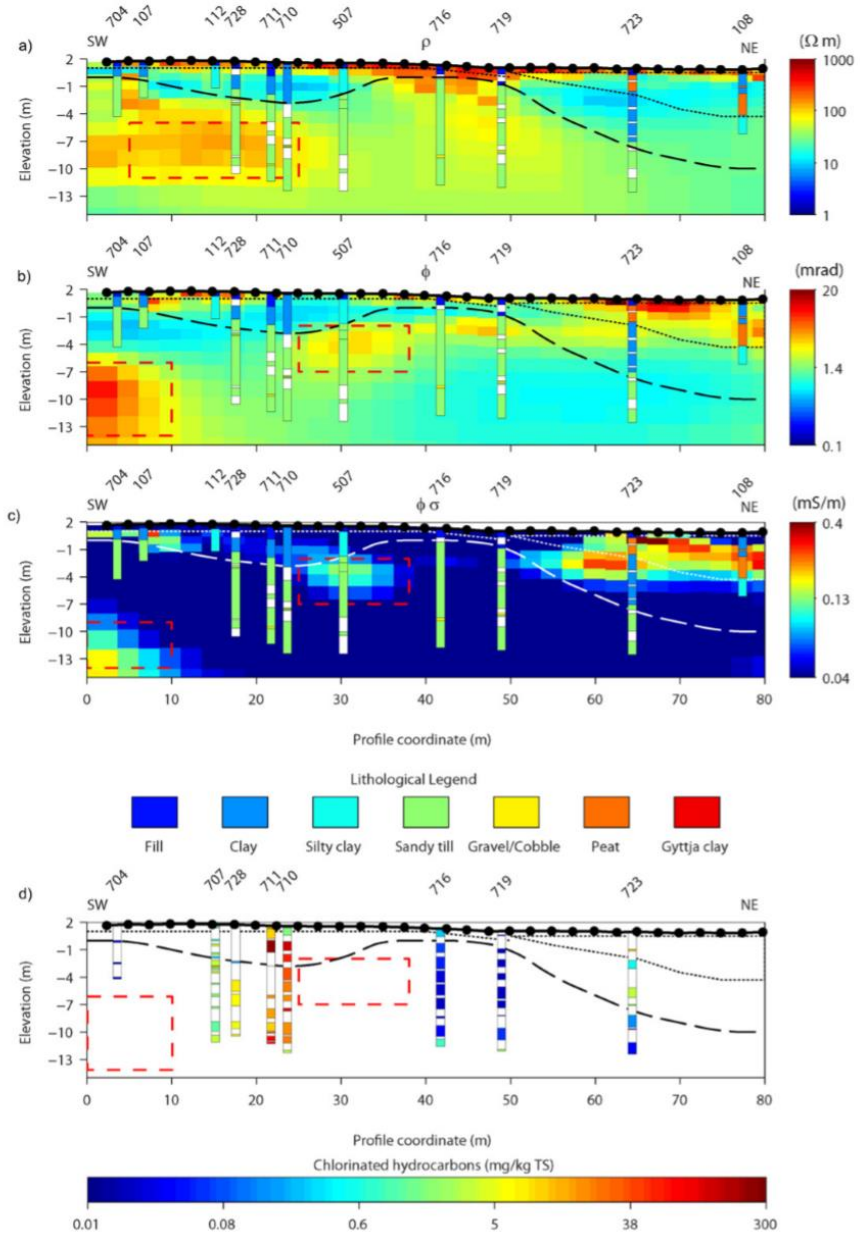

879

880

881 **FIGURE 7**

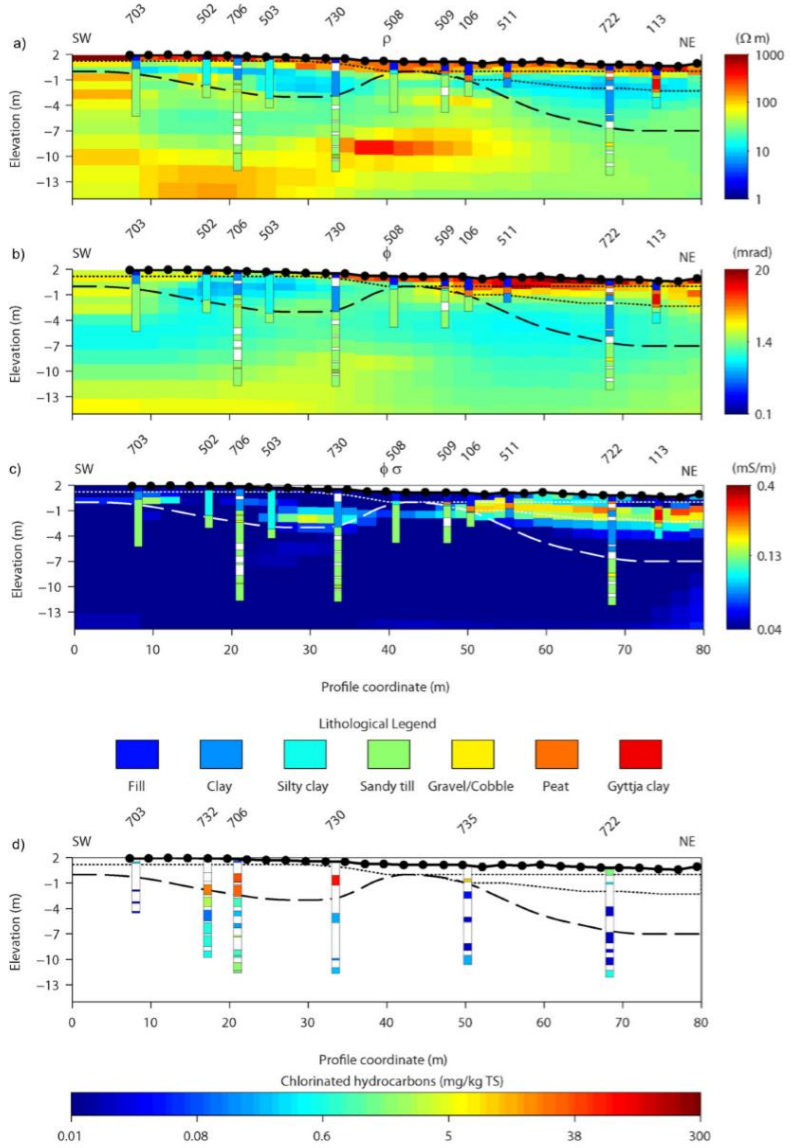

882

883

884 **FIGURE 8**

885

886

887 **FIGURE 9**

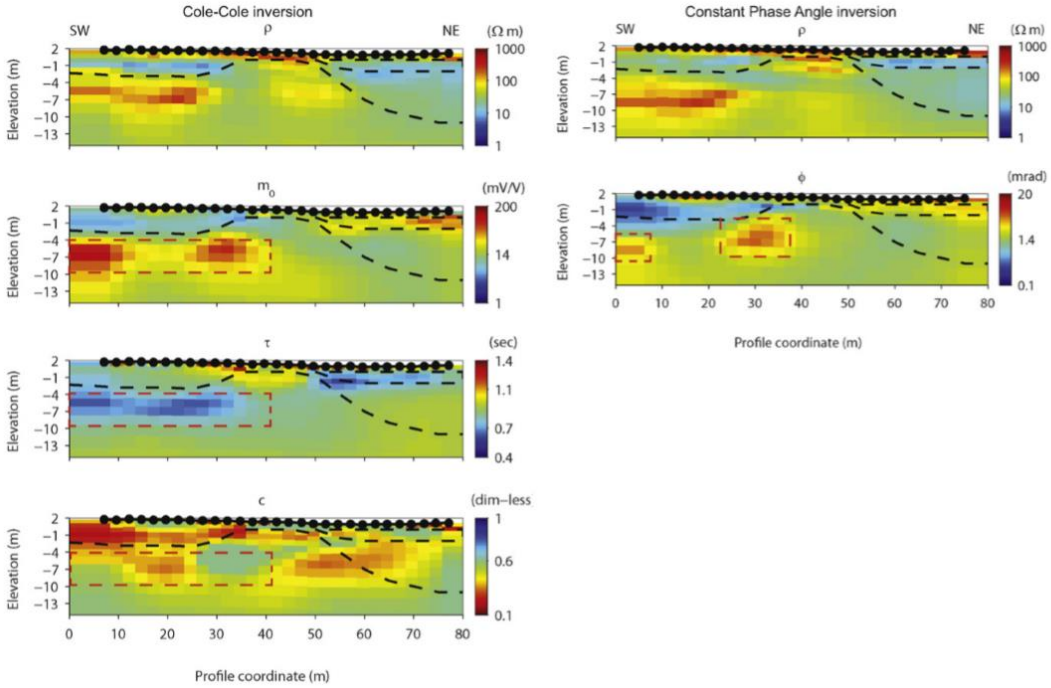

888

889

890 **FIGURE 10**

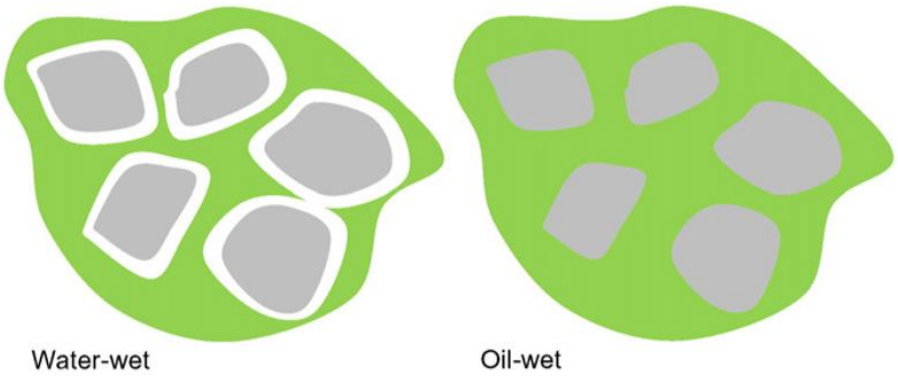

891

892

893 **FIGURE 11**

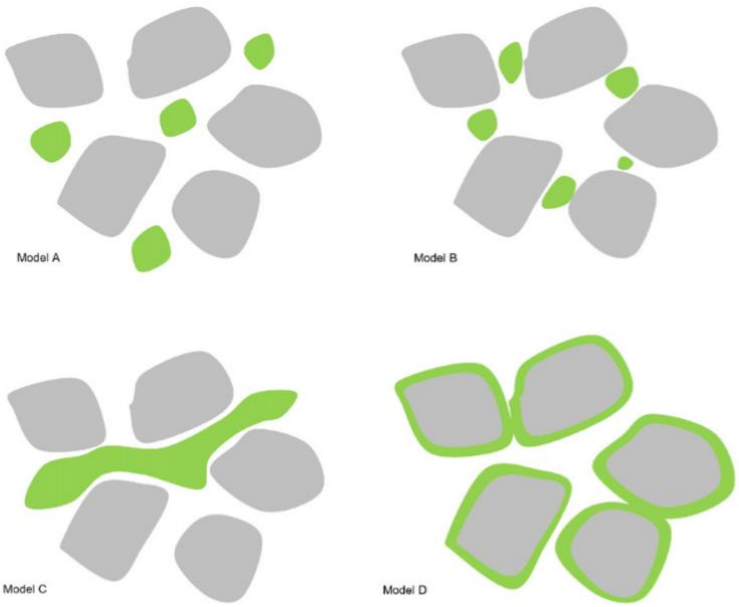

894